Analysis and Design Considerations of LLCC Resonant Multioutput DC/DC LED Driver With Charge Balancing and Exchanging of Secondary Series Resonant Capacitors

Xinke Wu, *Member, IEEE*, Chen Hu, Junming Zhang, *Senior Member, IEEE*, and Zhaoming Qian, *Senior Member, IEEE*

***Abstract*—A new rectifier for multioutput LED driver is proposed based on a charge exchanging and balancing principle in the secondary resonant capacitors. Combined with common ground rectifier and LLCC resonant topology, a four-output dc–dc LED driver is proposed with minimum quantity of secondary charge balancing capacitors. In the LLCC topology, the secondary side resonant capacitors can be used as dc blocking and charge balancing capacitors. The proposed LED driver can automatically share the average output currents by the charge balancing and exchanging among secondary resonant capacitors. The operating principle and the brief design guidelines for the four-output LLCC resonant dc–dc converter are presented. The guaranteed current sharing capability of the proposed four-output LED driver is also analyzed thoroughly. Finally, a 150 W four outputs LLCC resonant dc–dc LED driver is built-up to verify the theoretical analysis.**

***Index Terms*—Charge balancing, charge exchanging, current sharing, LED driver, LLCC resonant, multioutput.**

I. Introduction

In recent years, high-brightness LED has been widely used in many applications, such as street lighting, automobiles, and backlighting, for its high luminous efficacy, long lifetime, etc. The maximum current rating of individual LED module is limited by packaging technology and thermal management. Most applications require a large number of LEDs in a single system to achieve expected luminance value [1], [2]. Because the forward current of LED luminous quantity determines its luminance, it is important to keep the current in each LED identical for the same luminance and exotherm [3]. The series connecting structure is the easiest way to balance the current in LEDs. But, this results in high bus voltage and poor reliability. Therefore, using LED strings in parallel has been a common practice [4]. But the current sharing ability is poor in LEDs because the LED's exponential voltage–current characteristic and the negative temperature coefficient of its forward voltage drop, current balancing technique is necessary in multistring LEDs.

One method to achieve current sharing of paralleled LED strings is using a linear or switching circuit to form a current post regulator in each string. With linear regulator [4]–[8], the power loss is a major problem even employing bus voltage adaptive control especially when the voltage differences of the LED strings are high. With the switching-mode post regulator [9]–[13], the efficiency can be improved by sacrificing the cost. Another method is using the passive components like capacitive or magnetic components to attain current sharing capability. The current sharing transformer-based method is simple and low cost [14]–[20], [32], but the magnetic component is usually bulky. Furthermore, it introduces additional power loss and needs custom design for different output specifications. The capacitor impedance-based method [21], [33] needs high impedance capacitance which causes high reactive power and circulating energy in LED driver. Moreover, the current sharing accuracy is low when the LED's voltage drops of multistrings are different. In [22]–[25], a charge balancing principle in capacitor is simple, precise, and low cost to achieve precise current sharing. However, one capacitor can only realize current sharing between two LED strings, and additional magnetic components have to be introduced for more LED strings [25], [26].

Based on the charge balance principle, literatures [27]–[30] presented multichannel LED drivers based on charge balancing in secondary blocking capacitors without additional magnetic components. These structures inherit the advantages of the charge balancing method and can be easily extended to multistring LED lighting applications with charge exchanging between the blocking capacitors. An isolated dual-output dc–dc LED driver composed of an LLCC resonant inverter was discussed in [23]. With the second resonant capacitor at secondary side, the current overshoot in LED strings at dynamic and the size of the capacitor can be reduced. In this paper, an LLCC resonant dc–dc LED driver with multiple secondary resonant capacitors and multioutput is proposed. This paper puts emphasis on the circuit derivation, operating principle, and current

Manuscript received December 4, 2013; revised January 21, 2014; accepted February 25, 2014. Date of publication March 4, 2014; date of current version October 7, 2014. This paper was supported in part by grants from the Power Electronics Science and Education Development Program of Delta Environmental and Educational Foundation and the Fundamental Research Funds for the Central Universities (No. 2013QNA4022). Recommended for publication by Associate Editor J. M. Alonso.

The authors are with the College of Electrical Engineering, Zhejiang University, Hangzhou, Zhejiang 310027, China (e-mail: wuxinke@zju.edu.cn; huchen@zju.edu.cn; zhangjm@zju.edu.cn; qian@zju.edu.cn).

Color versions of one or more of the figures in this paper are available online at http://ieeexplore.ieee.org.

Digital Object Identifier 10.1109/TPEL.2014.2309605

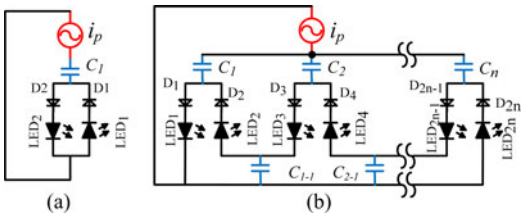

Fig. 1. Multioutput LED driver with charge balancing method. (a) Dual outputs [21], [22]. (b) Multiple outputs [29].

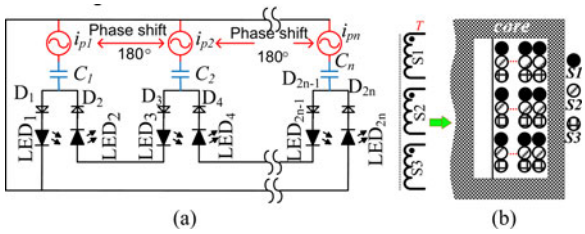

Fig. 2. Improved multioutput LED driver with minimum capacitors. (a) Circuit structure. (b) Winding structure.

sharing capability of the multiple outputs LLCC dc–dc LED driver.

II. Multioutput Circuits Derivations by Utilizing Charge Balance

Fig. 1(a) shows a simple two-output driver using the charge balancing principle of capacitance [22], [23]. Based on the charge balance and charge exchanging, a multioutput rectifier can be derived in Fig. 1(b) [29].

With intermediate capacitors C_{1-1}, C_{2-2}, etc., the neighboring LED strings can be connected directly by inserting an intermediate capacitor. For multiple output rectifiers, more capacitors are needed. In order to reduce the number of capacitors, a current source i_p is split into multiple sources with 180° phase shift between neighboring current sources shown in Fig. 2. The amount of secondary blocking capacitor is reduced significantly compared to the circuit in Fig. 1(b). Although more current sources are needed, they can be implemented by multiple windings in one transformer. The structure is shown in Fig. 2(b) for the purpose of reducing the leakage inductance among secondary windings. The multiwinding transformer for circuit in Fig. 1(b) is also necessary in order to avoid circulating current when common-ground rectifier is used.

In practical applications, the LED strings are connected with common ground because of the control system and safety requirements. A simple dual-output rectifier with common ground was proposed in [22]. Using a split bridge rectifier, two LED strings can be connected with the common ground and controlled with one current reference signal. By integrating the method in Fig. 3 and the multioutput rectifier in Fig. 2, an improved four-output rectifier with common ground is constructed in Fig. 4, where three capacitors are needed to achieve the charge balance among outputs. For the purpose of comparing the size and cost of multioutput LED drivers with charge balance technique, the numbers of key components of previous topologies

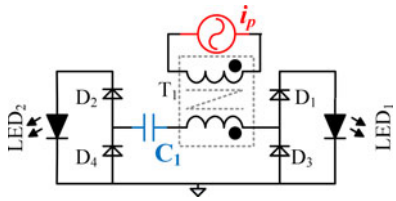

Fig. 3. Common ground dual-output rectifier [22], [23].

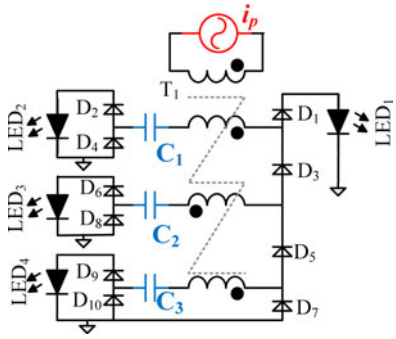

Fig. 4. Four-output common-ground rectifiers [30].

TABLE I
Components Comparison Among Topologies With Common Ground Outputs

	[26]	[29]	[21, 33]	Proposed
Number of Output capacitor	4	4	4	4
Number of Rectifying diodes	8	12	8	10
Number of Charge balancing capacitor	2	5	2	3
Number of Current sharing transformer	1	0	0	0
Number of Secondary windings	2	3	2	3
Current sharing performance	Good	Perfect	Medium	Perfect

with common ground outputs are listed in Table I. The number of components of the proposed converter is low and the current sharing performance is perfect owing to the charge balancing principle.

Because the capacity of each capacitor depends on the primary inverter topology, in order to reduce the size and cost of the series blocking capacitors, a multioutput resonant LLCC converter is proposed where the series blocking capacitors are used as the resonant components. Hence, the secondary side charge balancing capacitors are parts of resonant tank of the LLCC resonant converter. A four-output half-bridge LLCC resonant converter with proposed multioutput rectifier is shown in Fig. 5, whose outputs have common ground. The capacity of balancing capacitor can be reduced to the similar value of primary side resonant capacitor. In order to achieve dc output currents in LED strings, the output capacitance of each output is large enough. Hence, the output can be assumed to be voltage source during a switching cycle. There is a resonant capacitor C_r and a resonant inductance L_r at primary side. The magnetizing

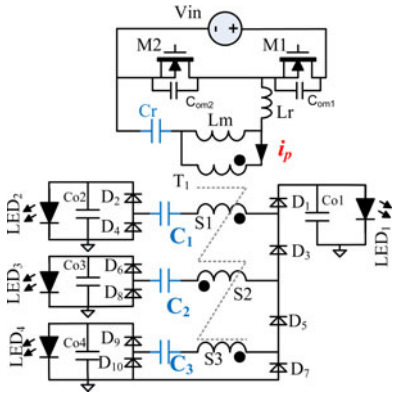

Fig. 5. Proposed four-output LLCC resonant LED driver.

inductance L_m of transformer is utilized as the second resonant inductance. The secondary side resonant capacitors are C_1, C_2, and C_3. The turns ratios of three secondary windings S_1, S_2, and S_3 are the same.

III. Operating Principle of the Four Outputs LLCC Resonant Converter

Since the secondary side capacitors are integrated into the series resonant tank, namely, the primary capacitor is in series with the secondary side capacitors. Therefore, the series resonant frequency is determined by the equivalent capacity of series connected C_r and reflected secondary side capacitor. According to the relationship between the switching frequency f_s and the first series resonant frequency f_r, whose resonant tank includes L_r, C_r, C_1, C_2, and C_3, the circuit operating condition can be divided into continuous current mode (CCM, $f_s \geq f_r$) and discontinuous current mode (DCM, $f_s < f_r$).

The key waveforms are shown in Fig. 6 for DCM and CCM operations. And, the corresponding equivalent circuits of DCM and CCM operating condition are shown in Figs. 7 and 8, respectively. For both CCM and DCM operating conditions, the operation in half switching cycle can be divided into three modes in terms of the switching transition and the currents waveforms in the transformer windings. Detailed circuit operations of each mode during half switching cycle are described as following.

A. DCM Condition

Mode 1 [t_0–t_1]: This mode begins when primary switch M_2 turns OFF at t_0. Current i_{Lr} in the resonant inductance L_r equals the magnetizing current i_{Lm} of L_m. Therefore, the current i_p keeps at zero. Because magnetizing inductance L_m is large enough, it can be seen as a current source in this interval and charges the intrinsic capacitances C_{om1} and C_{om2} of M_1 and M_2, who are assumed to be line capacitances during this interval. The equivalent circuit of this mode is shown in Fig. 7(a). This mode ends when the voltage v_{dsM2} across M_2 reaches V_{in}.

Mode 2 [t_1–t_2]: When voltage v_{dsM2} reaches V_{in}, the secondary side diodes D_1, D_4, D_5, D_6, and D_{10} begin to conduct. Because the current i_{Lr} is negative, it flows through the body diode of M_1 after t_1, which creates the zero voltage switching (ZVS) condition for M_1. Hence, M_1 is turned ON with ZVS. Then, the resonance between inductor L_r and capacitors C_r, C_1, C_2, and C_3 begins. During this interval, the outputs V_{O1}, and V_{O4} are charged by the current i_{S1} and i_{S2}, respectively. This mode ends when current i_{Lr} reaches i_{Lm} again. The equivalent circuit of this mode is shown in Fig. 7(b).

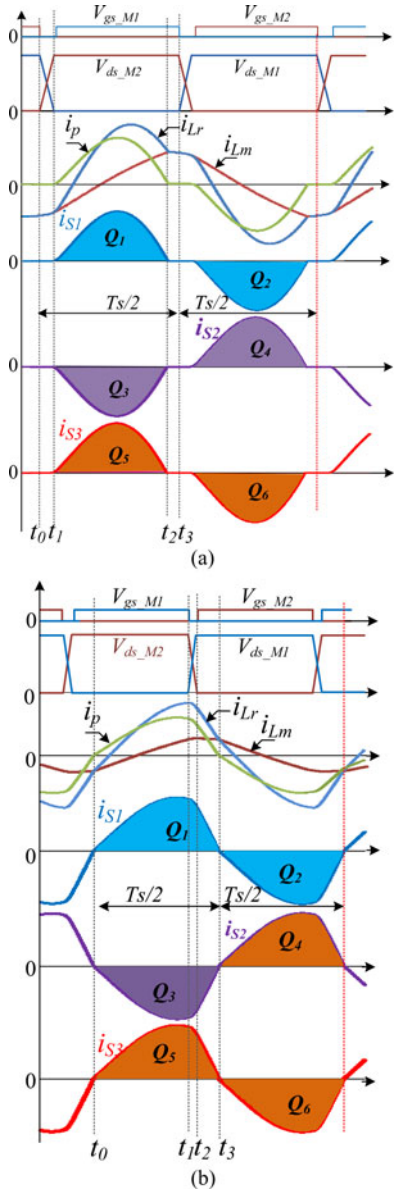

Fig. 6. Key waveforms of the proposed four-output LLCC resonant converter. (a) DCM. (b) CCM.

Mode 3 [t_2–t_3]: Since switching frequency f_s is lower than the series resonant frequency f_r, when the current i_{Lr} reaches i_{Lm} at t_2, the secondary side diodes are off and the magnetizing inductance L_m joins into the second series resonant tank, which includes L_r, L_m, C_r, C_1, C_2, and C_3 and whose resonant frequency is much less than the first resonant frequency f_r. This mode ends when primary switch M_1 turns OFF at t_3. The equivalent circuit of this mode is shown in Fig. 7(c).

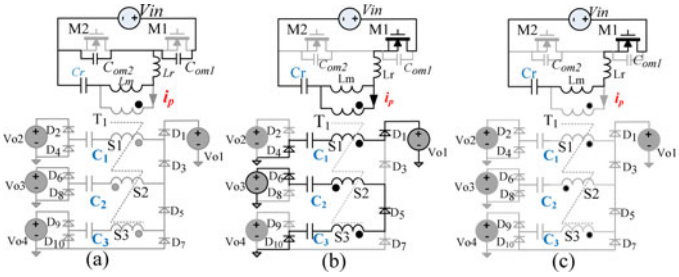

Fig. 7. Equivalent circuits of modes in DCM operation. (a) Mode 1(t_0-t_1). (b) Mode 2(t_1-t_2). (c) Mode 3(t_2-t_3).

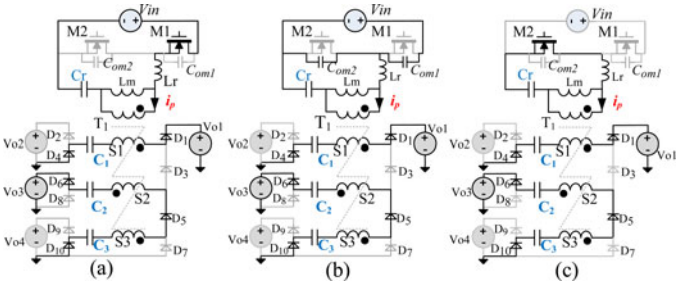

Fig. 8. Equivalent circuits of modes in CCM operation. (a) Mode 1(t_0-t_1). (b) Mode 2(t_1-t_2). (c) Mode 3(t_2-t_3).

After t_3, primary switch M_1 is turned OFF and the next half cycle begins. The next half switching period is similar to earlier description because of the symmetry of the circuit. During next half cycle, the outputs V_{O2} and V_{O4} are charged by i_{S1} and i_{S3}, respectively.

B. CCM Condition

Mode 1 [t_0–t_1]: Since switching frequency f_s is higher than the series resonant frequency f_r, when the current i_{Lr} reaches i_{Lm} at t_0, the secondary side diodes D_2, D_3, D_7, D_8, and D_9 are off, and diodes D_1, D_4, D_5, D_6, and D_{10} begin conducting. The primary capacitor C_r and inductance L_r resonant with secondary side capacitors C_1, C_2, and C_3. This mode ends when primary switch M_1 turns OFF at t_1. The equivalent circuit of this mode is shown in Fig. 8(a).

Mode 2 [t_1–t_2]: After t_1, because the diodes D_1, D_4, D_5, D_6, and D_{10} are still on, the resonant inductance L_r charges the intrinsic capacitances of M_1 and M_2 during this interval. The equivalent circuit of this mode is shown in Fig. 8(b). This mode ends when the voltage v_{dsM1} across M_1 reaches V_{in}.

Mode 3 [t_2–t_3]: When voltage v_{dsM1} reaches V_{in} at t_2, the current i_{Lr} flows through the body diode of M_2, which creates the ZVS turn-on condition for M_2. Hence, M_2 is turned ON after t_2 and ZVS on is achieved. This mode ends when current i_{Lr} reaches i_{Lm}, and diodes D_1, D_4, D_5, D_6, and D_{10} are off. The equivalent circuit of this mode is shown in Fig. 8(c).

After t_3, the diodes D_2, D_3, D_7, D_8, and D_9 begin to conduct. The next half switching cycle is similar to earlier operations except that the polarity of the currents reverses because of the symmetrical operation of the converter.

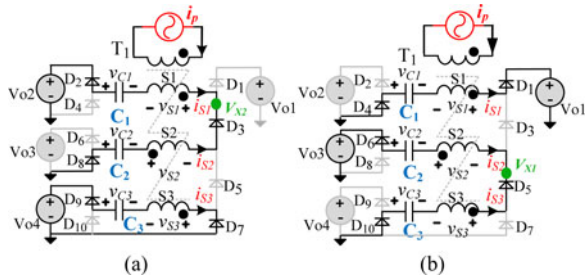

Fig. 9. Simplified equivalent circuits with an ac current source i_p in one switching cycle. (a) Charging interval. (b) Discharging interval.

C. Brief Introduction of Current Sharing Principle

Because the current sharing is achieved by the charge balancing principle of secondary resonant capacitor occurred in whole switching cycle, one switching cycle should be considered. During the half switching cycle (t_0-t_3) of both operating condition the charge should be equal to the charge in the other half switching period for each series secondary capacitor, as described in (1). Besides, C_2 and C_3 are connected in series in the first half switching period, thus $i_{S2}=i_{S3}$. Hence, Q_3 equals Q_5. Similarly, $i_{S1}=i_{S2}$ in the second half cycle, hence, Q_2 is identical to Q_4 as described in (2). Because of the large capacity of output capacitors, the currents in LED strings LED_1, LED_2, LED_3, and LED_4 are the average values of Q_1, Q_2, Q_3, and Q_6 over the switching period T_s in (3), where $T_s = 1/f_s$. According to (1), (2), and (3), the output current of each LED string is identical and the current sharing is achieved:

$$\begin{cases} Q_1 = \int_0^{Ts/2} i_{\mathrm{S1}}dt = Q_2 = \int_{Ts/2}^{Ts} i_{\mathrm{S1}}dt \\ Q_3 = \int_0^{Ts/2} i_{\mathrm{S2}}dt = Q_4 = \int_{Ts/2}^{Ts} i_{\mathrm{S2}}dt \\ Q_5 = \int_0^{Ts/2} i_{\mathrm{S3}}dt = Q_6 = \int_{Ts/2}^{Ts} i_{\mathrm{S3}}dt \end{cases} \tag{1}$$

$$\begin{cases} Q_3 = \int_0^{Ts/2} i_{\mathrm{S2}}dt = Q_5 = \int_0^{Ts/2} i_{\mathrm{S3}}dt \\ Q_2 = \int_{Ts/20}^{Ts} i_{\mathrm{S1}}dt = Q_4 = \int_{Ts/2}^{Ts} i_{\mathrm{S2}}dt \end{cases} \tag{2}$$

$$I_{\mathrm{LED}} = I_{\mathrm{LED1}} = Q_1/Ts = I_{\mathrm{LED2}} = Q_2/Ts = I_{\mathrm{LED3}} = Q_3/Ts = I_{\mathrm{LED4}} = Q_6/Ts. \tag{3}$$

IV. Design Considerations

A. Simplification of the Proposed Four-Output LLCC Converter

In order to simplify the analysis of current sharing capability and obtain the design guidelines of secondary side resonant capacitors, the primary side can be modeled as a high frequency ac current source i_p. Whatever it is continuous or discontinuous as depictured in earlier sections, there are a charging interval and a discharging interval for each secondary side capacitor in one switching cycle.

From Fig. 9(a), according to Kirchhoff's voltage law, (4) can be derived. And (5) can be derived from the discharging interval

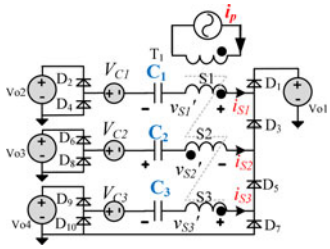

Fig. 10. Equivalent circuit where the dc components are separated from the secondary series resonant capacitors.

of Fig. 9(b):

$$\begin{cases} v_{\mathrm{S}2}(t) - v_{C3}(t) + v_{C2}(t) + v_{\mathrm{S}3}(t) = V_{O3} \\ v_{\mathrm{S}1}(t) - v_{C1}(t) = V_{O1} \end{cases} \tag{4}$$

$$\begin{cases} v_{\mathrm{S}2}(t) - v_{C2}(t) + v_{C1}(t) + v_{\mathrm{S}1}(t) = V_{O2} \\ v_{\mathrm{S}3}(t) + v_{C3}(t) = V_{O4}. \end{cases} \tag{5}$$

The average values of the winding voltages $v_{\mathrm{S}1}(t)$, $v_{\mathrm{S}2}(t)$, and $v_{\mathrm{S}3}(t)$ in half cycle are defined in (6). Because the duty cycles of charging and discharging intervals are almost the same and the turns ratios of secondary side windings are equal owing to their high coupling factors in Fig. 2(b), according to the volt–second balance of the secondary windings during two intervals, the average values of $v_{\mathrm{S}1}(t)$, $v_{\mathrm{S}2}(t)$, and $v_{\mathrm{S}3}(t)$ in charging and discharging intervals are the same $V_{\mathrm{S}1} = V_{\mathrm{S}2} = V_{\mathrm{S}3} = V_{\mathrm{S}}$:

$$\begin{cases} \int_0^{Ts/2} v_{\mathrm{S}1}(t)dt = V_{\mathrm{S}1} = \int_{Ts/2}^{Ts} v_{\mathrm{S}1}(t)dt \\ \int_0^{Ts/2} v_{\mathrm{S}2}(t)dt = V_{\mathrm{S}2} = \int_{Ts/2}^{Ts} v_{\mathrm{S}2}(t)dt \\ \int_0^{Ts/2} v_{\mathrm{S}3}(t)dt = V_{\mathrm{S}3} = \int_{Ts/2}^{Ts} v_{\mathrm{S}3}(t)dt. \end{cases} \tag{6}$$

Therefore, by replacing $v_{\mathrm{S}1}(t)$, $v_{\mathrm{S}2}(t)$, and $v_{\mathrm{S}3}(t)$ in (4) and (5) with V_s, the average values of the voltages across C_1, C_2, and C_3 can be derived as follows:

$$\begin{cases} V_{\mathrm{C}1} = -\dfrac{5V_{O1} - V_{O2} - V_{O3} - V_{O4}}{6} \\ V_{\mathrm{C}2} = \dfrac{V_{O3} + V_{O4} - V_{O1} - V_{O2}}{6} \\ V_{\mathrm{C}3} = \dfrac{5V_{O4} - V_{O1} - V_{O2} - V_{O3}}{6} \end{cases} \tag{7}$$

where V_{C1}, V_{C2}, and V_{C3} are the average voltages of C_1, C_2, and C_3, respectively. The average voltages can be separated from the capacitors and be defined as the dc voltages sources V_{C1}, V_{C2}, and V_{C3}, separately, shown in Fig. 10. Hence, only ac components, namely the voltage ripples on C_1, C_2, and C_3, are remained on the capacitors. Then, in order to simplify the circuit further, three virtual voltages $v_{\mathrm{S}1}{}'(t)$, $v_{\mathrm{S}2}{}'(t)$, and $v_{\mathrm{S}3}{}'(t)$ are defined as shown Fig. 10. The voltage $v_{\mathrm{S}1}{}'(t)$ is the voltage across the secondary winding S_1 and the capacitor C_1 without dc voltage component, as well as $v_{\mathrm{S}2}{}'(t)$ is across S_2 and C_2 and $v_{\mathrm{S}3}{}'(t)$ is across S_3 and C_3.

Obviously, because the outputs are dc voltages, $v_{\mathrm{S}1}{}'(t)$, $v_{\mathrm{S}2}{}'(t)$, and $v_{\mathrm{S}3}{}'(t)$ are square-wave voltages. And, they can

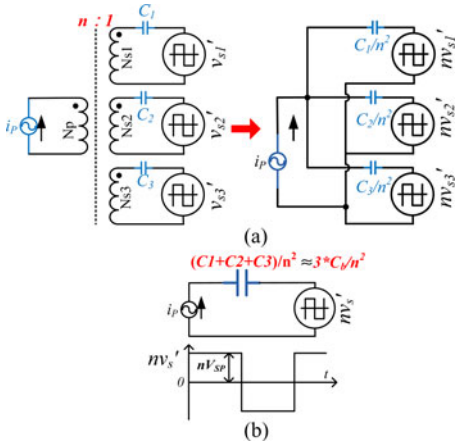

Fig. 11. Simplified equivalent circuit.

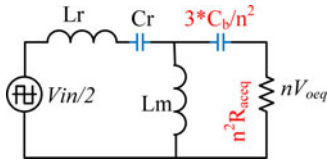

Fig. 12. AC equivalent circuit of single output LLCC converter.

be equalized to three parallel outputs shown in Fig. 11(a). Since the equivalent capacitors C_1/n^2, C_2/n^2, and C_3/n^2 are almost the same, the amplitude of three virtual outputs $n^* v_{S1}{}'(t)$, $n^* v_{\mathrm{S}2}{}'(t)$, and $n^* v_{\mathrm{S}3}{}'(t)$ are equal, where n is the turns ratio of the transformer $n = \mathrm{Np}/\mathrm{N}_{\mathrm{S}1}$. Therefore, they can be merged into one output $n^* v_S{}'(t)$ shown in Fig. 11(b), where $\mathrm{n}^* V_{SP}$ is the amplitude of $n^* v_S{}'(t)$ and $\mathrm{C}_b = \mathrm{C}_1 \approx \mathrm{C}_2 \approx \mathrm{C}_3$. From (7) and the equivalent circuit in Fig. 10 and the discharging interval in Fig. 9(b), the amplitude V_{SP} can be derived as follows:

$$n \cdot V_{SP} = n\left(\frac{V_{O1} + V_{O2} + V_{O3} + V_{O4}}{6}\right). \tag{8}$$

According to the equivalent circuit in Fig. 11(b), the equivalent output voltage is defined as $V_{\mathrm{oeq}} = \frac{V_{O1}+V_{O2}+V_{O3}+V_{O4}}{6}$. Since the average current in half switching cycle for each secondary winding is I_{LED} from (3), the equivalent total output current of three parallel windings is $6^* I_{\mathrm{LED}}$. Hence, the equivalent load is defined as $R_{\mathrm{eq}} = V_{\mathrm{oeq}}/(6^* I_{\mathrm{LED}})$.

After the four-output LLCC converter is simplified into single output converter, the fundamental harmonic approximation is used to simplify the analysis of LLCC converter by referring to the analysis methodology of LLC converter [31]. Fig. 12 shows the equivalent circuit of the single output LLCC resonant converter [23].

The equivalent ac resistance R_{aceq} can be deduced in

$$R_{\mathrm{aceq}} = \frac{4}{3\pi^2}\frac{V_{\mathrm{oeq}}}{I_{\mathrm{LED}}}. \tag{9}$$

In terms of the simplified equivalent circuit in Fig. 12, the steady-state voltage gain of the LLCC resonant dc–dc converter

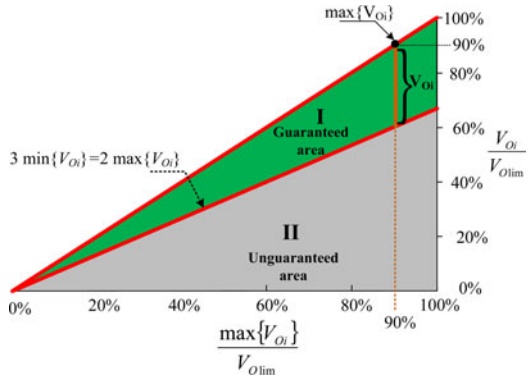

Fig. 13. Ranges of current sharing capability for the proposed four-output LED driver.

can be derived as follows:

$$G=\frac{n\cdot V_{oeq}}{\frac{V_{in}}{2}}$$

$$=\left|\frac{Z_1}{z_1+\frac{1}{j\cdot 2\pi\cdot f_s\cdot C_r}+j\cdot 2\pi\cdot f_s\cdot L_r}\cdot\frac{n^2\cdot R_{aceq}}{\frac{n^2}{j\cdot 2\pi\cdot f_s\cdot C_b}+n^2\cdot R_{aceq}}\right| \tag{10}$$

where $Z_1=j\cdot 2\pi\cdot f_s\cdot L_m//\left(\frac{n^2}{j\cdot 2\pi\cdot f_s\cdot C_b}+n^2R_{aceq}\right)$.

In the practical design procedure of an LED driver, the steady-state output of the converter is controlled to be a dc current source by the output current control loop. Hence, the output current in LED strings is constant and the output voltages for LED strings depend on the voltage drop of LED strings.

B. Output Voltage Range of Current Sharing Capability

As mentioned in Section II, transformer windings S_2 and S_3 are in series in the first half cycle. But, there is a restriction that voltage V_{X1} shown in Fig. 9(a) in charging mode meets (11), otherwise diodes D_3 or D_7 would conduct, which leads to $i_{s2}\neq i_{s3}$. Similarly, voltage V_{X2} shown in Fig. 9(b) in discharging mode should meet (12). Combined with (4), voltages V_{X1} and V_{X2} can be solved in (13). Then, four inequalities for the restrictions of the output voltage can be concluded in (14)–(17). The set of inequalities can be used to judge and design the output voltage ranges with guaranteed current sharing capability:

$$0\le V_{X1}\le V_{O1} \tag{11}$$

$$0\le V_{X2}\le V_{O1} \tag{12}$$

$$\begin{cases} V_{X1}=V_{S3}-V_{C3}=\dfrac{V_{O1}+V_{O2}+V_{O3}-2V_{O4}}{3} \\ V_{X2}=-V_{S2}-V_{C2}=\dfrac{2V_{O1}+2V_{O2}-V_{O3}-V_{O4}}{3} \end{cases} \tag{13}$$

$$V_{O1}+V_{O2}+V_{O3}\ge 2\cdot V_{O4} \tag{14}$$

$$2\cdot V_{O1}+2\cdot V_{O4}\ge V_{O2}+V_{O3} \tag{15}$$

$$V_{O1}+V_{O3}+V_{O4}\ge 2\cdot V_{O2} \tag{16}$$

$$2\cdot V_{O1}+2\cdot V_{O2}\ge V_{O4}+V_{O3}. \tag{17}$$

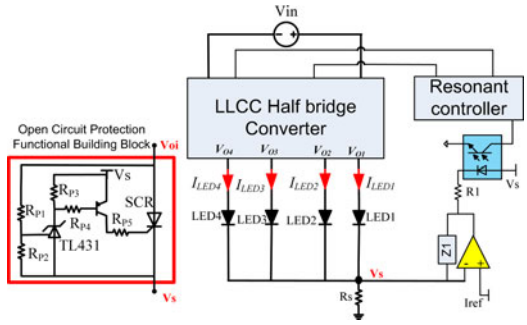

Fig. 14. Output current control strategy for four-string LEDs.

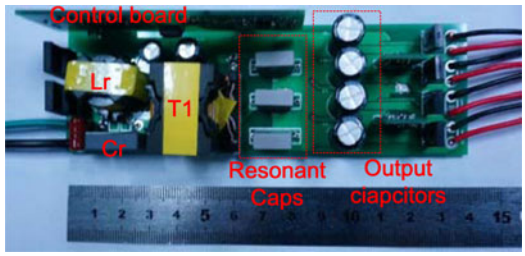

Fig. 15. Photo of the prototype.

TABLE II
KEY PARAMETERS OF THE PROTOTYPE

Parameters		Parameters	
fr	70 kHz	**Lr**	257 uH
Np: Ns1: Ns2:Ns3	n=2.55	**Cr**	33 nF
Lm	803 uH	**C_1, C_2, C_3**	100 nF
MOSFETs	FDP12N50/	**Diodes**	MBRS3201

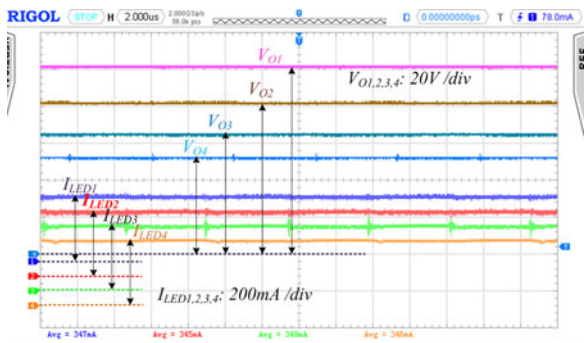

Fig. 16. Output voltages and currents of four LED strings (350 mA/channel).

In practical applications, the voltage deviations of four LED strings are mainly caused by the voltage tolerances of LED modules and temperature variations. Hence, the voltage deviations among the outputs are random. In order to meet the randomness of LED voltage variations, the available voltage rangeof each output should be the same. For the purpose of evaluating the current sharing capability, we define the minimum real-time output voltage among outputs as $\min\{V_{Oi},\ i=1,2,3,4\}$ and the maximum real-time output voltage as $\max\{V_{Oi},\ i=1,2,3,4\}$. The

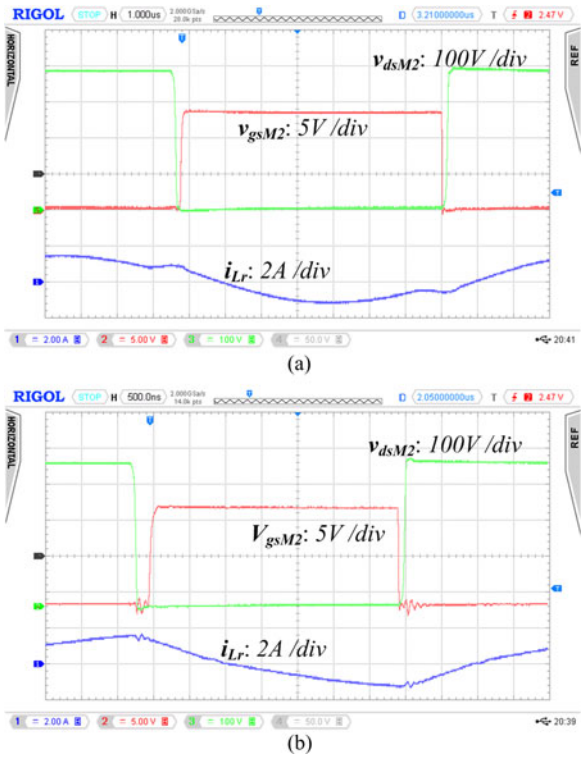

Fig. 17. Switching waveforms of primary switches and currents (gate, drain to source voltage and primary current). (a) DCM. (b) CCM mode.

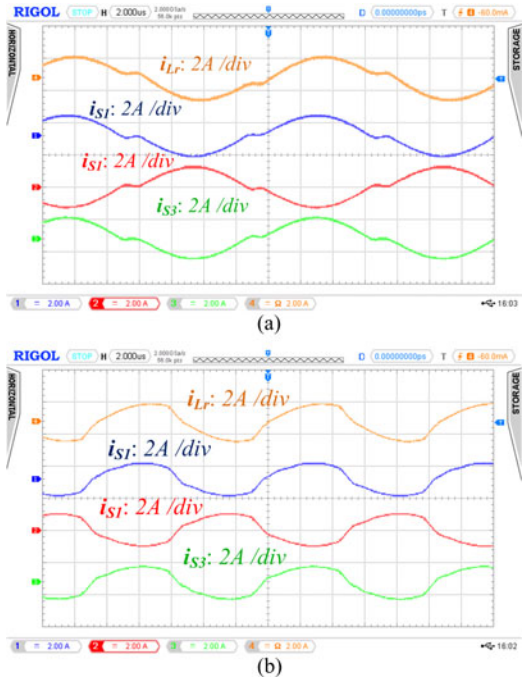

Fig. 18. Currents flowing though the transformer windings. (a) DCM. (b) CCM.

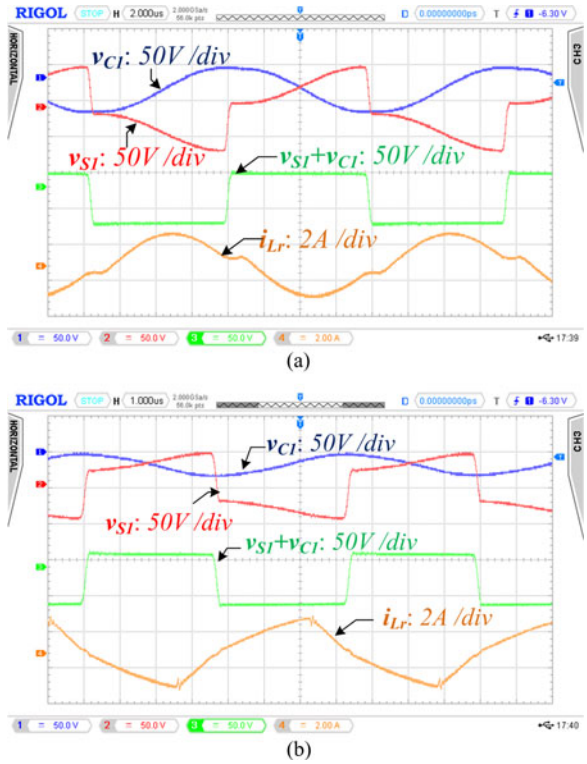

Fig. 19. Voltages across C_1 and transformer winding S_1. (a) DCM. (b) CCM.

worst condition for inequalities (14) and (16) is that the variables on the left equal to $\min\{V_{Oi,i=1,2,3,4}\}$ and the variable on the right is $\max\{V_{Oi,i=1,2,3,4}\}$.With this condition, if the output voltages can meet (14) and (16), they are easy to match the inequalities (15) and (17). Then, inequality (18) is derived for the guaranteed current sharing ability from (14) and (16). It should be noticed that when some of the output voltages beyond this range, the current sharing ability have to be judged based on the set of inequalities of (14) to (17) because the inequality (18) is a sufficient condition for current sharing capability among four outputs. From (18), the guaranteed current sharing condition can be depictured in Fig. 13:

$$3 * \min\{V_{Oi,i=1,2,3,4}\} \geq 2 * \max\{V_{Oi,i=1,2,3,4}\}. \quad (18)$$

By defining another variable, the maximum output voltage limitation, as V_{Olim}, the guaranteed current sharing voltage area (region I) of the proposed topology can be depictured in Fig. 13, where the ratio of maximum real-time output voltage $\max\{V_{Oi,i=1,2,3,4}\}$ over the specified maximum output V_{Olim} is used as the horizontal axis, the ratio of each real-time output voltage V_{Oi} over V_{Olim} is used as the vertical axis. For the guaranteed region I, the lower edge means the minimum output $\min\{V_{Oi}\}$ equals 2/3 of $\max\{V_{Oi}\}$, which presents the critical condition of inequality (18). For example, when the $\max\{V_{Oi}\}$ is 90% of V_{Olim}, a vertical line can be plotted. The cross point of upper edge of region I and the vertical line is the $\max\{V_{Oi}\}$. When other three outputs are located in the solid section of the vertical line, the current sharing ability is guaranteed. However, if there are other outputs at the dashed section, the current sharing is not guaranteed. The region II is unguaranteed area for current sharing ability, where the current sharing ability has to be verified by the set of inequalities from (14) to (17). With

TABLE III
MEASURED OUTPUT CURRENTS AT DIFFERENT OUTPUT VOLTAGES

Case	V_{O1}(V)	V_{O2}(V)	V_{O3}(V)	V_{O4}(V)	I_{LED1}(mA)	I_{LED2}(mA)	I_{LED3}(mA)	I_{LED4}(mA)	Region
A	99.7	99.6	99.6	99.8	340	339	340	340	**I**
B	49.8	49.7	49.6	49.7	340	339	340	340	**I**
C	79.1	55.1	55.1	55.0	340	339	340	340	**I**
D	55.1	79.1	55.1	55.0	340	339	340	340	**I**
E	84.9	55.1	55.1	55.0	340	339	340	340	**II**
F	55.5	84.5	55.6	55.6	366	311	366	366	**II**

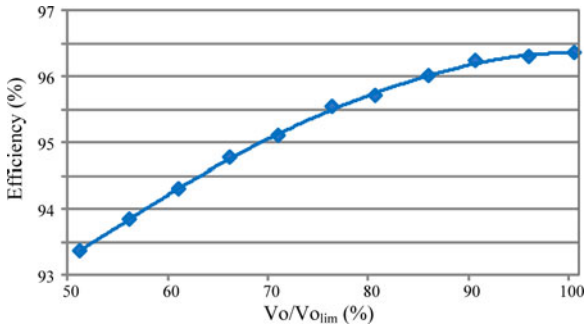

Fig. 20. Measured efficiency versus different output voltages ($V_{\mathrm{O}\lim}$ = 100 V).

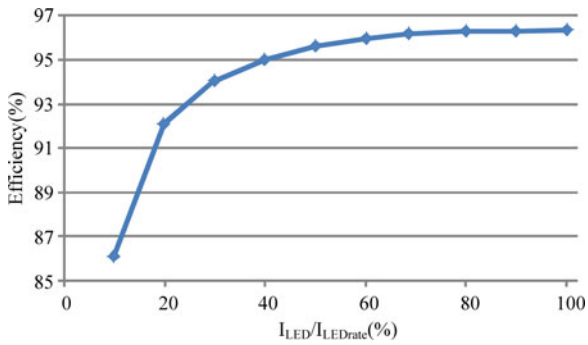

Fig. 21. Measured efficiency versus LED current when all output voltages equal $V_{\mathrm{O}\lim}$.

Fig. 13, the current sharing range can be designed when the maximum output voltage max$\{V_{Oi}\}$ is determined.

V. EXPERIMENTAL VERIFICATIONS

To verify the analysis of the proposed LLCC resonant multioutput LED driver, a laboratory prototype with 50 V–100 V/350 mA (I_{LEDrate} = 350 mA) for each output was built and tested. The total output current is controlled by a current feed-back loop to regulate resonant frequency of LLCC stage as shown in Fig. 14. An open-circuit protection circuit is used to prevent voltage overshoot, which is the same to [30]. The prototype photo is shown in Fig. 15. The key parameters of the prototype are given in Table II. The dc voltage stress of the secondary resonant capacitors at normal condition is $V_{\mathrm{O}\lim}/2$, which can be calculated according to (7) by considering the current sharing range in Fig. 13. Therefore, taking into account the switching frequency ripple at full power, the voltage rating of the capacitors in this prototype is less than 200 V.

With the control scheme in Fig. 14, the output voltages are determined by the voltage drop of LED strings because the total output current is controlled. In order to demonstrate the current sharing ability, the counts of LED module for each string are different. Hence, the output voltages are different as shown in the measured results of Fig. 16, i.e., V_{O1} = 99 V, V_{O2} = 85 V, V_{O3} = 63 V, and V_{O4} = 50 V. The average currents in all LED strings are almost identical.

The gate signal and drain to source voltage of M_2 is shown in Fig. 17. ZVS turn-on is achieved at both operating conditions, DCM and CCM. Because the CCM operating condition appears when the equivalent output voltage is much lower than rated value, therefore, the output power decreases. The currents flowing through the primary winding and three secondary windings of the transformer are given in Fig. 18. Both DCM and CCM operating modes are provided. The amplitudes of the current waveforms in secondary side windings are identical, which guarantees the average output current the same. The voltages across the secondary winding S_1 and secondary capacitor C_1 are shown in Fig. 19. There is not only dc voltage, but also switching voltage ripple on the capacitor C_1, which will affect the voltage across the transformer. The voltage sum of v_{C1} and $v_{\mathrm{S}1}$ are also measured in Fig. 19. Owing to the existing of dc voltage on C_1, volt-second of the voltage sum of v_{C1} and $v_{\mathrm{S}1}$ is unbalanced and its average value is the dc components on C_1.

Table III lists measured average output currents and voltages of four outputs at six load conditions. When the output voltages are in the region I of Fig. 13, current sharing is achieved (cases A, B, C, and D). While, when the voltages of LED strings are out of guaranteed current sharing region (case F), current balancing could not be achieved. However, in some cases, the current sharing capability could be achieved. For example, although case E is in region II, the current sharing is still achieved because the output voltage conditions match the inequalities in (14)–(17). A failure mode, open circuit, has been demonstrated in [30] with a protection circuit. This protection circuit (functional building block) can be used in the prototype of this paper. When open circuit happens in one of LED strings, the protection circuit works and the LED string will be shorted. Hence, the output voltage of the open-circuit string will be zero and the converter enters in unguaranteed range when protection circuit works. Therefore, the current sharing capability should be judged according to the inequalities (14)–(17).

Finally, the efficiency of the prototype is measured when four outputs are the same, in that the efficiency depends on

the equivalent output voltage and current. The efficiency curve versus different output voltages is given in Fig. 20, where the load current is 350 mA/string. For the purpose of demonstrating the efficiency when the output current is dimmed, the efficiency curve with different LED current is also given in Fig. 21, when all the output voltages are V_{Olim} and I_{LEDrate} is 350 mA.

VI. Conclusion

An improved multioutput rectifier with charge balance in the secondary side resonant capacitors is presented and analyzed in this paper. It utilizes charge balance in the secondary resonant capacitors and series–parallel autoregulated connection of secondary windings to realize current sharing among LED strings. With this concept, the amount of secondary balancing capacitor can be minimized. Using this rectifying concept and the common ground rectifier, an LLCC resonant dc–dc LED driver with four common ground outputs is constructed, where three balancing capacitors are needed for four outputs. The average currents of different LED strings are identical even the voltage difference among the LED strings are large. Because no additional magnetic components are introduced, the proposed structure is simple, lossless. The design guideline for the output voltage range with guaranteed current sharing capability is provided. The experimental results on the four-output LED prototype verify the analysis and design guidelines.

References

[1] Y. K. Cheng and K. W. E. Cheng, "General study for using LED to replace traditional lighting devices," in *Proc. 2nd Int. Conf. Power Electron. Syst. Appl.*, Nov. 12–14, 2006, pp. 173–177.

[2] M. Krames, O. Shchekin, R. Mueller-Mach, G. Mueller, L. Zhou, G. Harbers, and M. Craford, "Status and future of high-power light emitting diodes for solid-state lighting," *Display Technol. J.*, vol. 3, no. 2, pp. 160–175, Jun. 2007.

[3] Y.-C. Li and C.-L. Chen, "A novel single-stage high-power-factor AC-to-DC LED driving circuit with leakage inductance energy recycling," *IEEE Trans. Ind. Electron.*, vol. 59, no. 2, pp. 793–802, Feb. 2012.

[4] C. Chen, C. Wu, Y. Chen, and T. Wu, "Sequential color LED backlight driving system for LCD panels," *IEEE Trans. Power Electron.*, vol. 22, no. 3, pp. 919–925, May 2007.

[5] H. Chiu and S. Cheng, "LED backlight driving system for large-scale LCD panels," *IEEE Trans. Ind. Electron.*, vol. 54, no. 5, pp. 2751–2760, Oct. 2007.

[6] Y. Hu and M. Jovanovic, "LED driver with self-adaptive drive voltage," *IEEE Trans. Power Electron.*, vol. 23, no. 11, pp. 3116–3125, Mar. 2008.

[7] S. K. Ng, K. H. Loo, S. K. Ip, Y. M. Lai, C. K. Tse, and K. T. Mok, "Sequential variable bilevel driving approach suitable for use in high-color-precision LED display panels," *IEEE Trans. Ind. Electron.*, vol. 59, no. 12, pp. 4637–4645, Dec. 2012.

[8] S. Li, Z. W. X. Zhong, W. Chen, and S. Y. R Hui, "Novel self-configurable current-mirror techniques for reducing current imbalance in parallel light-emitting diode (LED) strings," *IEEE Trans. Power Electron.*, vol. 27, no. 4, pp. 2153–2162, Apr. 2012.

[9] H. Chiu, Y. Lo, J. Chen, S. Cheng, C. Lin, and S. Mou, "A high-efficiency dimmable LED driver for low-power lighting applications," *IEEE Trans. Ind. Electron.*, vol. 57, no. 2, pp. 735–743, Feb. 2010.

[10] Q. Hu and R. Zane, "LED driver circuit with series-input-connected converter cells operating in continuous conduction mode," *IEEE Trans. Power Electron.*, vol. 25, no. 3, pp. 574–582, Mar. 2010.

[11] W. Chen and S. Y. R. Hui, "A dimmable light-emitting diode (LED) driver with Mag-Amp post-regulators for multi-string applications," *IEEE Trans. Power Electron.*, vol. 26, no. 6, pp. 1714–1722, Jun. 2011.

[12] H. Chen, Y. Zhang, and M. Dongsheng, "A SIMO parallel-string driver IC for dimmable LED backlighting with local bus voltage optimization and single time-shared regulation loop," *IEEE Trans. Power Electron.*, vol. 27, no. 1, pp. 452–462, Jan. 2012.

[13] W. Yu, J.-S. Lai, H. Ma, and C. Zheng, "High-efficiency DC–DC converter with twin bus for dimmable LED lighting," *IEEE Trans. Power Electron.*, vol. 26, no. 8, pp. 2095–2100, Aug. 2011.

[14] Y. Hu and M. M. Jovanović, "A new current-balancing method for paralleled LED strings," in *Proc. IEEE 26th Annu. Conf. Appl. Power Electron. Conf. Expo.*, Mar. 2011, pp. 705–712.

[15] S. M. Baddela and D. S. Zinger, "Parallel connected LEDs operated at high frequency to improve current sharing," in *Proc. IEEE 39th IAS Annu. Meet. Conf. Ind. Appl. Conf.*, Oct. 2004, vol. 3, pp. 1677–1681.

[16] W. Thomas and J. Pforr, "A novel low-cost current-sharing method for automotive LED-lighting systems," in *Proc. 13th Eur. Conf. Power Electron. Appl.*, 2009, pp. 1–10.

[17] K. I. Hwu and S. Chou, "A simple current-balancing converter for LED lighting," in *Proc. IEEE Appl. Power Electron. Conf.*, 2009, pp. 587–590.

[18] S. Ji, H. Wu, X. Ren, and F. C. Lee, "Multi-channel constant current (MC3) LED driver," in *Proc. IEEE Appl. Power Electron. Conf.*, 2011, pp. 718–722.

[19] Z. Wang, X. Wu, M. Chen, and J. Zhang, "Optimal design methodology for the current-sharing transformer in a quasi-resonant (QR) flyback LED driver," in *Proc. IEEE 27th Annu. Conf. Appl. Power Electron. Conf. Expo.*, Feb. 2012, pp. 2372–2378.

[20] X. Wu, Z. Wang, and J. Zhang, "Design considerations for dual-output quasi-resonant flyback LED driver with current-sharing transformer," *IEEE Trans. Power Electron.*, vol. 28, no. 10, pp. 4820–4830, Oct. 2013.

[21] S. Choi and T. Kim, "Symmetric current-balancing circuit for LED backlight with dimming," *IEEE Trans. Ind. Electron.*, vol. 59, no. 4, pp. 1698–1707, Apr. 2012.

[22] X. Wu, J. Zhang, and Z. Qian, "A simple two-channel LED driver with automatic precise current sharing," *IEEE Trans. Ind. Electron.*, vol. 58, no. 10, pp. 4783–4788, Oct. 2011.

[23] Y. Chen, X. Wu, and Z. Qian, "Analysis and design considerations of LLCC resonant DC–DC converter with precise current sharing for two-channel LED driver," in *Proc. IEEE Energy Convers. Congr. Expo.*, 2011, pp. 2771–2776.

[24] J. Zhang, L. Xu, X. Wu, and Z. Qian, "A precise passive current balancing method for multi-output LED drivers," *IEEE Trans. Power Electron.*, vol. 26, no. 8, pp. 2149–2159, Aug. 2011.

[25] J. Zhang, J. Wang, and X. Wu, "A capacitor-isolated LED driver with inherent current balance capability," *IEEE Trans. Ind. Electron.*, vol. 59, no. 4, pp. 1708–1716, Apr. 2012.

[26] Y. Zhang, C. Hu, and X. Wu, "Analysis and design of LLCC resonant four-channel DC–DC LED driver with current sharing transformer," in *Proc. IEEE 28th Annu. Conf. Appl. Power Electron. Conf. Expo.*, Feb. 2013, pp. 3295–3300.

[27] S. Zhang, Q. Chen, J. Sun, X. Ming, and Q. Yang, "High-accuracy passive current balancing schemes for large-scale LED backlight system," in *Proc. IEEE 26th Annu. Appl. Power Electron. Conf. Expo.*, 2011, pp. 723–727.

[28] S. H. Cho, S. H. Lee, S. Hong, D.-S. Oh, and S.-K. Han, "High-accuracy and cost-effective current-balanced multichannel LED backlight driver using single-transformer," in *Proc. IEEE 8th Int. Conf. Power Electron. ECCE Asia*, 2011, pp. 520–527.

[29] C. Zhao, X. Xie, and S. Liu, "Multi-output LED drivers with precise passive current balancing," *IEEE Trans. Power Electron.*, vol. 28, no. 3, pp. 1438–1448, Mar. 2013.

[30] X. Wu, C. Hu, J. Zhang, and C. Zhao, "Series–parallel auto-regulated charge-balancing rectifier for multi-output light-emitting diode driver," *IEEE Trans. Ind. Electron.*, vol. 61, no. 3, pp. 1262–1268, Mar. 2014.

[31] B. Yang, F. C. Lee, A. J. Zhang, and G. Huang, "LLC resonant converter for front end DC/DC conversion," in *Proc. IEEE 17th Annu. Appl. Power Electron, Conf. Expo.*, 2002, pp. 1108–1112.

[32] R. Zhang and H. S. H. Chung, "Use of daisy-chained transformers for current-balancing multiple LED strings," *IEEE Trans. Power Electron.*, vol. 29, no. 3, pp. 1418–1433, Mar. 2014.

[33] K. H. Loo, Y. M. Lai, and C. K. Tse, "Design and analysis of LCC resonant network for quasi-lossless current balancing in multi-string AC-LED array," *IEEE Trans. Power Electron.*, vol. 28, no. 2, pp. 1047–1059, Feb. 2013.

Xinke Wu (M'10) received the B.S. and M.S. degrees in electrical engineering from Harbin Institute of Technology, China, in 2000 and 2002, respectively, and the Ph.D. degree in electrical engineering from Zhejiang University, Hangzhou, China, in 2006.

He was a Postdoctoral Fellow of the National Engineering Research Center for Applied Power Electronics in Zhejiang University from 2007 to 2009, and was an Assistant Research Fellow from 2009 to 2010. Since 2011, he has been an Associate Professor in electrical engineering with Zhejiang University. From 2011 to 2012, he was a Visiting Scholar in the Center of Power Electronics System, Virginia Tech. His research covers high efficiency LED driving technology, soft switching and high efficiency power conversion, and power electronics system integration.

Dr. Wu was awarded Distinguished Young Scholar of Zhejiang University in 2012.

Chen Hu was born in Zhejiang, China, in 1987. He received the B.S. degree in electrical engineering from Zhejiang University, Hangzhou, China, in 2008, where he is currently working toward the Ph.D. degree in electrical engineering.

His current research interests include LED driver and high-efficiency dc/dc converters.

Junming Zhang (M'10–SM'13) received the M.S. and Ph.D. degrees in electrical engineering from Zhejiang University, Hangzhou, China, in 2000 and 2004, respectively.

He is an Associate Professor of the College of Electrical Engineering in Zhejiang University. His research interests include power electronics system integrations, power management, dc/dc converter, synchronous rectifier and high power inverters.

Zhaoming Qian (SM'92) received graduate degree in radio engineering from the Electrical Engineering Department, Zhejiang University, Hangzhou, China, in 1961, and the Ph.D. degree in applied science from Catholic University of Leuven and the Interuniversity Microelectronics Center, Leuven, Belgium, in 1989.

Since 1961, he has been doing teaching and research work on electronics and power electronics in Zhejiang University of China. He was promoted as a Professor of the Electrical Engineering Department of Zhejiang University in 1992. He is currently the Deputy Director of the National Engineering Research Center for Applied Power Electronics at Zhejiang University and the Deputy Director of Scientific Committee, National Key Laboratory of Power Electronics at Zhejiang University. His main professional interests include power electronics and its industrial applications, power electronic system integration, and EMC in power electronic systems, etc. He has published one book on EMC design and more than 200 papers.

Dr. Qian received Excellent Education Awards from the China Education Commission and from Zhejiang University, in 1993, 1997, and 1999, respectively, the Science and Technology Development Awards from the China Education Commission, in 1999 and 2003, respectively.